Processes and patterns: Insights on cranial covariation from an Apert syndrome mouse model

Nandini Singh, Yann Heuzé, Gregory L. Holmes

Processes and Patterns: Insights On Cranial Covariation from An Apert Syndrome Mouse Model

NANDINI SINGH[1*], YANN HEUZÉ[2], GREG HOLMES[3]

[1]Department of Anthropology, California State University, Sacramento, CA

[2] Université de Bordeaux, CNRS, MC, PACEA, UMR5199, Pessac, France

[3]Department of Genetics and Genomic Sciences, Icahn School of Medicine at Mount Sinai, New York, NY

*****Corresponding author: Nandini Singh, 6000 J Street, Dept of Anthropology, CSUS. Sacramento CA 95819. E-mail: nandini.singh@csus.edu; Phone: (916) 278-5446

Running title: Cranial integration in Apert Syndrome

Keywords: Morphological integration, Fgfr2 S252W, geometric morphometrics, partial-least squares, modularity

Supported in part by grants from the NIH: NICHD R01-HD038384; NIDCR R01-DE018500, R01-DE018500-S2, R01-DE022988; and NIAMS AR051358

Abstract

Background: Major cell-to-cell signaling pathways, such as the fibroblast growth factors and their four receptors (FGF/FGFR), are conserved across a variety of animal forms. FGF/FGFRs are necessary to produce several "vertebrate-specific" structures, including the vertebrate head. Here, we examine the effects of the FGFR2 S252W mutation associated with Apert syndrome on patterns of cranial integration. Our data comprise micro-computed tomography images of newborn mouse skulls, bred to express the Fgfr2 S252W mutation exclusively in either neural crest or mesoderm-derived tissues, and mice that express the Fgfr2 S252W mutation ubiquitously.

Results: Procrustes-based methods and partial least squares analysis were used to analyze craniofacial integration patterns. We found that deviations in the direction and degree of integrated shape change across the mouse models used in our study were potentially driven by the modular variation generated by differing expression of the *Fgfr2* mutation in cranial tissues.

Conclusions: Our overall results demonstrate that covariation patterns can be biased by the spatial distribution and magnitude of variation produced by underlying developmental-genetic mechanisms that often impact the phenotype in disproportionate ways.

Introduction

Morphological integration and modularity describe the interdependence among different biological structures. Integration and its counterpart modularity can be studied as both patterns of integration and the strength of association among those units. At the phenotypic level, craniofacial integration manifests as hierarchical interactions among bony elements, soft tissue elements, and shared spaces – all of which are influenced by the developmental processes that generate those structures. Integration-inducing mechanisms include common cell lineages, morphogenetic networks, skeletal growth patterns, and muscle activity, among others. Exploring processes that affect morphological integration among different traits can provide important insights into how developmental systems influence morphological variation and how changes in one region indirectly impact another, not only in normal development but also in a clinical context such as craniosynostosis.

Experimental animal systems have contributed immensely to our understanding of mammalian biology and evolution. In particular, mouse models for human diseases have revealed that signaling pathways such as those regulated by members of the fibroblast growth factor (FGF) family and their transmembrane receptors (FGFRs) are conserved across mammalian phylogenies.[1] Vertebrates are known to have the largest number of members of this gene family implicated in producing several "vertebrate-specific" phenotypes.[2] The importance of FGF/FGFR signaling in human skull development is demonstrated by the effects of mutations in FGFR genes that are associated with craniosynostosis conditions such as Apert, Crouzon and Pfeiffer syndromes.[3,4] Craniosynostosis is a complex developmental disorder defined by the premature closure of cranial vault sutures[3]. Sutures serve as growth centers in the skull and premature closure of the cranial vault sutures can severely affect craniofacial growth.[5]

Consequently, this can influence the way in which the cranial vault structurally interacts and morphologically integrates with other components of the skull, particularly the facial skeleton[6].

Model organisms used to study human development and disease provide unique insights into the mechanistic underpinning that link the genotype to aspects of the phenotype. Previous studies[6,7] underscore the important evolutionary and developmental roles of FGF/FGFR signaling in maintaining coordinated growth across different parts of the cranium. Martínez-Abadías et al.[6] emphasize the influence of the FGF/FGFR signaling axis on cranial integration, particularly in modulating the degree of covariance between skeletal structures. Accordingly, our study proposes to determine whether differential expression of the Fgfr2 S252W mutation during development of the cranium of *Fgfr2*$^{+/S252W}$ Apert syndrome mice causes deviations in patterns of integration that are largely considered evolutionarily conserved across different mammalian phylogenies. We build on these earlier findings by comparing data from three previously published Apert syndrome mouse models that conditionally express the *Fgfr2*$^{+/S252W}$ mutation in: 1) mesoderm-derived components; 2) neural crest-derived components; 3) and all cranial tissues. Because normal functioning of Fgfr2 is critical for cranial vault development, models that express the mutation conditionally are useful to examine region-specific effects of the *Fgfr2*$^{+/S252W}$ mutation on the variance-covariance structures in the cranium.

In a clinical context, studying the impact of aberrant signaling on cranial integration facilitates understanding of how the targeted effects of a mutation in one region indirectly affect the interaction among different structures. The relevance of applying the concept of morphological integration to understand manifestations of craniosynostosis phenotypes caused by targeted expression of the Fgfr2 S252W mutation is two-fold. First, it provides a quantitative framework to examine the structural interaction and relationship between skeletal regions. This

is particularly useful when trying to describe – from a phenotypic perspective - how aberrant *Fgfr2* signaling that results in the premature closure of cranial vault sutures affects or alters the association between the cranial vault and other parts of the skull. Second, as morphological integration explicitly focuses on the interdependence of traits, this approach can be utilized to design effective craniofacial surgeries and subsequent reconstruction therapies.

To this end, we address the question: how does the $Fgfr2^{+/S252W}$ mutation affect cranial integration in our three mouse models? We hypothesize the following: H1) mice that express the mutation conditionally in bones derived from mesoderm (neurocranial components) and those from neural crest (facial skeleton and frontal bone), respectively, will be distinct from mice that express the mutation ubiquitously and those that are unaffected. Exploring the morphological differences between the conditional mutants and mutants that express the Fgfr2 S252W mutation in all tissues of the body will help to clarify localized/modular versus ubiquitous effects of the mutation on the craniofacial skeleton. H2) mice that express the mutation in all tissues of the skull will present cranial integration identical to the non-mutant mice, and different from that of the conditional mutants. The underlying assumption of the latter hypothesis is that a ubiquitous mutation that affects the cells of all tissues in the cranium will not drastically alter the structural association between regions derived from mesoderm and neural crest. This hypothesis is partially supported by Martínez-Abadías et al.[8] where they found the pattern of integration to be similar between the neurocranium and face in the Fgfr2 S252W Apert syndrome mouse model, but not the degree of association (i.e. correlation) between the two regions. Our study aims to provide additional insights into how tissue-specific mutations in highly conserved signaling systems affect the structure of variance and covariation between the neurocranium and face.

Results

Overall cranial shape differences across the mouse strains

The mean shapes capture the overall morphology of the different mouse strains used in this study (Figure 2). The most pronounced differences in shape are between the *Fgfr*$^{+/S252W}$ and the unaffected mice, with the *Fgfr*$^{+/S252W}$ group exhibiting an overall dome-like rounded cranium and relatively downwardly deflected snout compared to the latter. This disparity in shape is also supported by a pairwise analysis of Procrustes distances (0.0910) between the *Fgfr*$^{+/S252W}$ and unaffected mice (Table 3). The most distinct changes between the conditional mutants comprise a fused coronal suture in the *Meso*$^{+/S252W}$ mice and a more inferiorly rotated snout in the *NC*$^{+/S252W}$ group (Figure 2). All groups are significantly different in shape as measured by pairwise analyses of Procrustes distances (Table 3), though, the *Meso*$^{+/S252W}$ mice and the non-mutants seem to be the most similar in shape as indicated by the distance measure (0.0369; Table 3). These results partially support H1 in that the conditional mutants are distinct from the full mutants. However, the *Meso*$^{+/S252W}$ mice are the least distinct from the unaffected littermates, suggesting some overlap in shape (further clarified by the PCA results below).

As a next step, we performed a PCA of all twenty-eight cranial landmarks to explore the overall variation and distribution of the different groups in shape space (Figure 3). In PC 1 vs PC 2, PC 1 (52.5%) captures the between-group variation in the sample with the *Fgfr*$^{+/S252W}$ mice being the most distinct along the positive end of PC 1, followed by the *NC*$^{+/S252W}$ mice. The unaffected mice occupy the negative end of PC 1 and group close to the *Meso*$^{+/S252W}$ mice (Figure 3A). Similarities in aspects of cranial shape between the *Meso*$^{+/S252W}$ and nonmutant mice are also indicated by the shortest pairwise Procrustes distance between the two groups (Table 3). Shape changes along PC 1 are driven by the dome shape neurocranium and retracted

snout of the *Fgfr*$^{+/S252W}$ mice on the positive end, and an overall low and elongated cranium of the unaffected mice on the negative end (Figure 3A). PC 2 (10.2%) captures the within-group variation among the *Meso*$^{+/S252W}$ mice and also partially separates them from the other strains. The negative end on PC2 – occupied by the *Meso*$^{+/S252W}$ mice - shows a superiorly deflected snout and a low cranial vault (Figure 3A). Positive scores on PC 2 capture a ventrally raised parietal region and a slightly inferiorly deflected snout. In the comparison between PC 1 vs PC 3 (7.6%), PC 3 further captures the within group variation in the *Meso*$^{+/S252W}$ and unaffected groups (Figure 3B). Shape changes along PC 3 mainly account for changes in the cranial vault, with is supero-inferiorly raised and infero-posteriorly extended parietal region on the positive end compared to a supero-inferiorly low and rostrally placed parietal region on the negative end. The latter is possibly driven by the cranial vault shape of the *Meso*$^{+/S252W}$ and *Fgfr*$^{+/S252W}$ mice on PC 3(Figure 3B). Results of the PCA elucidate the ways in which the mouse strains vary in their main shape features, and their direction and range of within-group variation.

Differences in direction of integrated shape change in Apert syndrome mouse models

We conducted 2B-PLS analyses to test H1 and H2. PLS analysis explores patterns and magnitude of integration between blocks of variables, in this case being the mesoderm- and neural crest-derived regions. We conducted the 2B-PLS analyses with and without the effects of allometry (Figures 4 & 5). The 2B-PLS analysis with size intact, captures subtle differences in the pattern of integrated shape change - as demonstrated by the relative position and direction of the group scatters - among the *Fgfr*$^{+/S252W}$, *NC*$^{+/S252W}$, and *Meso*$^{+/S252W}$ mice (Figure 5A; Table 4). Specifically, shape change along Block 1 does not correspond to an equivalent amount of change along Block 2 in our mouse models. For patterns of integration to be similar among groups,

changes in Block 1 should be equivalent to the variation along Block 2 across the sample. Moreover, if the Fgfr2 S252W mutation did not impact patterns of integration, the mutant mice would present the same pattern and direction of change as the nonumutants.

PLS 1 (94.9%) without correction for size shows partial overlap between the *Meso*$^{+/S252W}$ group and unaffected mice, but they differ slightly in their direction of associated shape change (Figure 5A). The *Fgfr*$^{+/S252W}$ and *NC*$^{+/S252W}$ mice are distinct from one another and the *Meso*$^{+/S252W}$ and the unaffected mice (Figure 5A). Conversely, when allometry is removed from the analysis there is overlap among all the mouse strains on PLS 1 (86%) (Figure 5D). The separation among the mouse models when size is part of the analysis (Figure 5A) is likely due to differences in allometric variation (i.e. size related shape changes) across the groups. Indeed, results of the multivariate regression analysis of all the cranial Procrustes coordinates on centroid size shows that size significantly (P-value <0.0001) predicts 23.17% of the total shape variation (Figure 4A). This is also true for the neurocranial and facial landmarks, where size significantly (P-value <0.0001) predicts 14.43% of the shape variation in the neurocranium and 31% of the shape variation in the face (Figure 4B & 4C). However, despite the overlap among the groups when size is not part of the analysis (Figure 5D), the mouse models still preserve slight differences in individual group trajectories, which is captured by the direction of the group scatters relative to the diagonal.

Shape changes along the negative scores of PLS 1 show a supero-inferiorly high cranial vault, driven mostly by variation at the superior and postero-inferior most points taken on the parietal bones (lmks 17 & 20; Figure 1) and a retracted anterior vault, as indicated by changes in the antero-medial most points on the parietal bone (lmks 15 & 18; Figure 1) (Figure 6A). These neurocranial changes (Block 1) are associated with an overall medio-laterally narrow face and

anteriorly extended snout (Block 2). The positive scores capture a supero-inferiorly low cranial vault and an anteriorly extended parietal bone, covarying with a medio-laterally expanded face (Figure 6A).

PLS 2 (Figure 5B & E) shows some separation between the *NC*$^{+/S252W}$ mice and the other groups, but the general direction of group scatter (i.e. trajectory of integrated shape change) is similar between the *NC*$^{+/S252W}$ and *Fgfr*$^{+/S252W}$ mice along this dimension. The *Meso*$^{+/S252W}$ mice differ in their direction of change, following more of a horizontal trajectory compared to the other strains. PLS 3 (Figure 5C & F) shows an interesting deviation between the PLS analyses. This dimension captures subtle shape differences between the *Meso*$^{+/S252W}$ mice and the other groups, particularly when size is removed from the analysis (Figure 5F). The *Fgfr*$^{+/S252W}$ mutants also show slight deviations in their direction of shape change. However, it is important to note that PLS 3 accounts for very little to negligible amount of the shape covariance in the sample, 0.7% (Figure 5C) and 1.8% (Figure 5F) and does not necessarily portray strong differences in patterns of integration.

Modular shape variation in the neurocranium and face differs across the mouse models

Given that our sample comprises mice that express activation of the mutation either locally or ubiquitously, we further examined how patterns of integration are impacted by within-block or localized shape variation caused by differential activation of the *Fgfr*$^{+/S252W}$ mutation across the mouse models. Figures 7A and B show the within-block changes in the neurocranium with and without allometric variation, respectively, along PLS 1 vs PLS 2. We did not include PLS 3 because the total covariance accounted for was less than 2%. Both analyses (Figures 7A & B) show some overlap among the mouse strains along PLS 1 in aspect of the neurocranium, but

the ordination of the group scatters as well as the degree of variation is different across all the mutants and the nonmutants. The $NC^{+/S252W}$ mice, which only express the mutation in the neural crest-derived regions, tend to cluster away from the other groups along both PLS 1 and PLS 2 regardless of the effects of size (Figure 7A & B). Figures 7C and D illustrate the within-block variation in the face along PLS 1 vs PLS 2. The analysis with allometry (Figure 7C) captures size-related shape variation and distinguishes the $NC^{+/S252W}$ and $Fgfr^{+/S252W}$ mice from the $Meso^{+/S252W}$ and the unaffecteds along PLS 1 and PLS 2. The analysis without allometry shows overlap among all the groups except for the $NC^{+/S252W}$ mice, which are separated from the others along PLS 2 (Figure 7D).

The overall differences in modular or within-block variation in the neurocranium and face across the mouse strains suggests that localized activation of the mutation causes differential phenotypic changes. Moreover, modular shape variation tends to distinguish the $NC^{+/S252W}$ mice more than the others in both the neurocranium and facial components, indicating that the activation of the mutation in the face causes more pronounced changes than when it is expressed only in the mesoderm. Differential degrees of shape change within the two regions can affect the structural association between them, shifting patterns of integration among the mutants, and between the mutants and nonmutants.[23]

Magnitude of integration between the neurocranium and face: size

The RV coefficient values (0.46) and correlations along each PLS axes were higher when size was part of the analyses (Table 4), suggesting that the correlation between the two blocks (i.e. neurocranium vs face) is potentially influenced by size. However, in a separate analysis with just the nonmutants (not shown here), the RV coefficient value decreased when size was part of

the analysis (Table 4). Low correlation values in the nonmutants possibly reflect aspects of growth patterns (i.e changes in size) at P0 where parts of the developing cranium are less integrated with each other to allow for postnatal size adjustments that are not disrupted by the mutation.[24–27] However, most importantly, the mutants showed higher RV values compared to the nonmutants regardless of the influence of size (Table 4), indicating that the the *Fgfr*$^{+/S252W}$ mutation increases the magnitude of integration between the neurocranium and face.

In summary, our findings show the *Fgfr*$^{+/S252W}$ and *NC*$^{+/S252W}$ mice to be the most distinct in their overall cranial shape variation and patterns of covariation, particularly the *NC*$^{+/S252W}$ group that only express the mutation in the neural crest regions (Figures 3 & 7; Table 3). The 2B-PLS results *partially* support H1 in that all mutants show slight distinctions from each other and the unaffected mice, not just the conditional mutants. The slight deviations in patterns of integration among the mouse models in our sample are likely driven by differing degrees of within-block shape variation caused by the *Fgfr2* mutation in the neurocranium and face, respectively. Our results also provide some evidence for rejecting H2 as the full mutants and non-mutants do not share the same pattern of integration as hypothesized. In addition, we found that the Fgfr2 S252W mutation and size variables increase the degree of integration between the neurocranium and face in the mutants (Table 4).

Discussion

Here we examined whether the Fgfr2 S252W mutation associated with Apert syndrome impacts cranial integration patterns in three mouse models that carry the mutation either conditionally or ubiquitously. Examining patterns of integration among modules can provide valuable insight into how complex structures grow and change as a response to underlying

genetic processes. In a clinical context, studying the impact of aberrant signaling on cranial integration facilitates understanding of how the targeted activation of a mutation in one region affects contiguous structures. As stated earlier, our results partially support H1 in that all the groups in our sample, not just the conditional mutants, exhibit slight differences in patterns of integration between the mesoderm- and neural crest-derived regions along the first three PLS axes (~98% of the total covariance in the sample). Deviations in integration patterns among the mouse models are likely caused by differing levels of within-in module variation generated by the mutation (Figure 7). Our results emphasize the need to examine the influence of within-block variation on patterns of integration as modular variation can impact the association between structures across different genotypes.[28] In craniosynostosis, understanding how localized aberrant signaling alters the way in which different parts of the skull grow, integrate, and covary can serve as a therapeutic guide for surgical manipulations.

Changes in trajectory of integrated shape change: variance and covariance

The mice used in this study exhibit distinct craniofacial dysmorphologies associated with Apert syndrome.[29] Overall cranial shape of the *Fgfr2*$^{+/S252W}$ and *NC*$^{+/S252W}$ mice are the most distinct as illustrated in Figure 3 (also see Table 3). In terms of patterns of integrated shape change between the mesoderm- and neural crest-derived regions, all the mouse models vary from one another to some extent across the first three PLS axes. Our findings differ from a previous study by Martínez-Abadías et al.[8] that found cranial integration in the neurocranium and face to be similar in the *Fgfr2*$^{+/S252W}$ mutants and their unaffected littermates. One reason for the discrepancy between our findings and Martínez-Abadías et al.'s[8] could be that they compared cranial integration between two Apert syndrome mouse models, *Fgfr2*$^{+/S252W}$ and *Fgfr2*$^{+/P253R}$,

whereas the focus on this study is only on *Fgfr2*$^{+/S252W}$. Moreover, our comparisons comprise conditional mutants with targeted activation of the mutation in specific tissues and not just full mutants. However, our results align with Martínez-Abadías et al. in showing that the Fgfr2 S252W Apert syndrome mutation increases the correlation between the neurocranium and face (Table 3), corroborating the implication that FGF/FGFR signaling is a covariance-generating mechanism in the skull.[8,30]

Both PLS analyses with and without the effects of size show differences in patterns of integration. The differences are more enhanced when size is a part of the analysis, demonstrating that allometry impacts cranial integration patterns and correlation between the structures (Table 4). While the overall results of the PLS analyses do not change whether or not size is part of the analysis, it is important to consider how the Fgfr2 S252W mutation affects growth (i.e. size changes) of and between structures, particularly when considering surgical interventions. This is relevant for Apert syndrome, and possibly for other craniosynostosis conditions, in that knowing how structures change in relation to one another during normal and abnormal development can assist in designing surgical treatments that enhance long-term outcomes.

Differential patterns of modular variation in the neurocranium and face

Modular shape variation tends to distinguish the *NC*$^{+/S252W}$ mice more so than the others in both the neurocranium and facial components, indicating that the activation of the mutation in the face causes more pronounced changes than when it is expressed only in the mesoderm. Normal growth and development of the facial primordia is a result of intricately coordinated series of morphogenetic events.[31] The majority of the molecular pathways directing facial morphogenesis regulate the behavior of neural crest cells.[31] For example, the role of FGF/FGFR

signaling, particularly signaling involved with *Fgfr1* and *Fgfr2*, has been implicated in neural crest migration, survival, proliferation and patterning of the facial epithelia and mesenchyme.[32] Some other intercellular pathways critical for mid-facial fusion and growth include BMP, HH and Wnt signaling, which interact with FGF/FGFR signaling during embryogenesis[33]. During development, even slight perturbations in covariance-generating mechanisms, such as the FGF/FGFR pathway, can alter the structure of variation in the face and, consequently, covariation with adjoining cranial modules.[28]

Although clinical diagnoses of syndromic craniosynostosis typically involve closure of calvarial sutures, midface dysgenesis is also a feature of craniosynostosis syndromes and mouse models of Apert and Crouzon craniosynostosis syndromes exhibit midface dysgenesis similar to the human conditions.[34] Specifically, Holmes et al.[34] showed that tissues impacted in the Apert $Fgfr2^{+/S252W}$ mutants included non-skeletal elements such as reduction in the volume of the nasal cavity associated by thickening of the nasal cartilages. Using morphological integration as a framework can facilitate the study of direct (within-region) and indirect (between-region) phenotypic manifestations of premature closure of cranial vault sutures. For instance, examining the combined effects of thickening of the nasal passages along with potential reduction in facial and cranial vault bone growth could provide insights into inter-tissue interactions between different parts of the cranium during normal and abnormal development and as it informs surgical procedures.

Conclusion

Morphological integration and the related concept of modularity describe the ways in which different modules or parts of an organism integrate to form a functioning system.

Conditional activation of the Fgfr2 S252W mutation in either mesoderm or neural crest-derived tissues provides a unique dataset to explore whether targeted variation in signaling alters the structural relationship between components of the skull. Our findings emphasize the impact of localized, modular genotypic effects on phenotypic variation and covariation patterns.

Experimental Procedures

Mouse models

The mice used in our study were bred, euthanized, processed, and imaged in compliance with animal welfare guidelines approved by the New York University and Pennsylvania State University Animal Care and Use Committees. The mice analyzed in this study were described in our previously published work. [7]

Our sample comprises a total of 116 newborn (P0) mutant mice and their non-mutant littermates (Table 1). The mutant mice were bred using a Cre-inducible Apert syndrome, the Fgfr2 S252W mutation. The different mutant groups in this study include: 1) P0 mice expressing the $Fgfr2^{S252W}$ allele in cranial components derived from mesoderm ($Meso^{+/S252W}$) and their unaffected littermates ($Meso^{+/+}$); 2) P0 mice expressing $Fgfr2^{S252W}$ in cranial components derived from neural crest cells ($NC^{+/S252W}$) and their unaffected littermates ($NC^{+/+}$); 3) P0 mice expressing the $Fgfr2^{S252W}$ allele in all tissues of the cranium ($Fgfr2^{+/S252W}$) and their unaffected littermates ($Fgfr2^{+/+}$). The mouse models used here have been previously described. [9,7] Briefly, all the mice in our sample were bred on a mixed background and heterozygous for a Cre. The mutant mice are all heterozygous for the floxed Fgfr2 S252W allele and the unaffected littermates are homozygous for the wild type *Fgfr2* allele. The mice were genotyped by PCR of

genomic DNA prepared from tail-snips for *Fgfr2*, *Neo* and *Cre*. For additional details are found here.[7]

Data and analyses

We analyzed twenty-eight cranial landmarks defined by their coordinate location in 3D space (Figure 1 and Table 2) measured on high-resolution micro computed-tomography (μCT) images of the mice in our sample. These landmarks were divided into regions derived from mesoderm (14 landmarks) and neural crest (14 landmarks).[11] All landmark data were collected by YH. Only landmarks that were consistently repeatable across our sample and measurement error free were included in the subsequent analyses.[7] The μCT images were acquired at the Center for Quantitative X-Ray Imaging at Pennsylvania State University, with a pixel size of 0.0135 x 0.0135mm and slice thickness of 0.0156mm. Image reconstruction was done on a pixel grid of 1024x1024 in 16 bit and reduced to 8 bit. Isosurfaces to represent all cranial bones were reconstructed from the 8 bit μCT images using the software package Avizo 6.3 (Visualization Sciences Group, VSG). Generalized Procrustes Analysis (GPA) was used to process the twenty-eight landmarks.[12] This method extracts shape coordinates from the original landmark data by translating, scaling, and rotating the data, subsequently yielding Procrustes shape coordinates. Centroid size (CS) is used as the measure for size, and is estimated as the square root of the sum of squared Euclidean distances from a set of landmarks to their centroid (i.e. "center of gravity – the average of the *x* and *y* coordinates of all landmarks). [13–15] All the specimens are scaled according to CS. The unaffected littermates of the respective mutants were combined for all subsequent analyses. The following statistical analyses were performed on Procrustes shape coordinates.

First, we computed Procrustes distances between the group means and performed a 1000 rounds of a two-sided permutation test.[16] In addition, we compared the mean shapes of the different mouse strains. Mean shapes represent the average shape of a sample, and were estimated based on the Procrustes coordinates of the different groups. Once computed, they were visualized on isosurfaces of the cranial CT-scans (details below).

Next, we performed a principal component analyses (PCA) of all the cranial landmarks used in this study to examine the overall shape variation across the different mouse models. This allows for a better understanding of how the *Fgfr2*$^{+/S252W}$ mutation affects global shape variation. PCA uses an eigenvalue decomposition of the covariance matrix resulting in mutually orthogonal dimensions assembled according to the amount of variance explained by each axis. Each axis represents a principal component that explains a portion of the variance in the dataset, with the first component accounting for the largest amount of variance in the sample.[17]

Last, we conducted a two-block partial-least squares (2B-PLS) analysis to examine the pattern of integration between regions derived from mesoderm (Block 1) and neural crest (Block 2) across all samples. The 2B-PLS method uses a singular value decomposition of the between-block covariance matrix yielding uncorrelated pairs of axes; the first pair accounting for the largest amount of covariance between the two blocks, the second for the second largest amount, and so on. This approach is commonly used to analyze morphological integration or covariation between two modules or blocks of variables defined *a priori*.[18] The 2B-PLS analysis was conducted on the Procrustes coordinates with the effects of allometry as well as on the regression residuals of the two blocks. The multivariate regression analyses were conducted on the Procrustes shape coordinates of the respective blocks (i.e. neurocranium and face) on the Centroid Size of the entire cranium.[15,19] We also conducted permutation tests associated with the

regression analyses, which used the null hypothesis of complete independence between the Procrustes coordinates (dependent variable) and centroid size (independent variable).

The reason for including both sets of PLS analyses was to examine possible effects of allometry on patterns and magnitude of shape covariation.[20] The landmarks for each block were subjected to separate Procrustes fits, and the covariation pattern between and within the two blocks was analyzed across the groups. In addition to the between-block association, we also examined within-block variation of the neurocranial and facial variables, respectively, along PLS 1 and PLS 2. This allows assessment of modular variation within each block along pairs of PLS axes. We also calculated the overall association or correlation between the blocks using the RV coefficient[21] that uses values from 0 to 1.0, 0 denoting complete independence between the two blocks.

One of the differences between PCA and 2B-PLS is that the latter orders the axes according to a measure of covariance explained by paired axes, not individual axes as in PCA. Employing both these analyses allows us to compare potential differences in patterns of covariation between the two blocks as well as overall cranial variation across our sample. Shape changes were visualized along the respective 2B-PLS axes via wireframe diagrams in MorphoJ.[22] All statistical analyses were performed in MorphoJ and R programming software. The μCT data used in this study are available on FaceBase. Landmark data are available on NS's website.

Acknowledgement

We thank Dr. Claudio Basilico for use of the mouse models analyzed here. We also thank Dr. Susan Motch Perrine, Tiffany Kim, and Hongseok Kim for managing and imaging the micro-

CT data. We are very grateful to Dr. Joan Richtsmeier for her insightful comments on earlier drafts of the manuscript. Supported in part by grants from the NIH: NICHD R01-HD038384; NIDCR R01-DE018500, R01-DE018500-S2, R01-DE022988; and NIAMS AR051358.

References

1. Coulier F, Pontarotti P, Roubin R, Hartung H, Goldfarb M, Birnbaum D. Of worms and men: an evolutionary perspective on the fibroblast growth factor (FGF) and FGF receptor families. *J Mol Evol*. 1997;44(1):43-56. doi:doi.org/10.1007/PL00006120

2. Bertrand S, Camasses A, Somorjai I, et al. Amphioxus FGF signaling predicts the acquisition of vertebrate morphological traits. *Proc Natl Acad Sci*. 2011;108(22):9160-9165. doi:10.1073/pnas.1014235108

3. Flaherty K, Singh N, Richtsmeier JT. Understanding craniosynostosis as a growth disorder. *Wiley Interdiscip Rev Dev Biol*. 2016;5(4):429-459. doi:doi.org/10.1002/wdev.227

4. Holmes G. The role of vertebrate models in understanding craniosynostosis. *Childs Nerv Syst*. 2012;28(9):1471-1481. doi:10.1007/s00381-012-1844-3

5. Opperman LA. Cranial sutures as intramembranous bone growth sites. *Dev Dyn*. 2000;219(4):472-485. doi:org/10.1002/1097-0177

6. Martínez-Abadías N, Heuzé Y, Wang Y, Jabs EW, Aldridge K, Richtsmeier JT. FGF/FGFR signaling coordinates skull development by modulating magnitude of morphological integration: evidence from Apert syndrome mouse models. *PLoS One*. 2011;6(10):e26425. doi:org/10.1371/journal.pone.0026425

7. Heuzé Y, Singh N, Basilico C, Jabs EW, Holmes G, Richtsmeier JT. Morphological comparison of the craniofacial phenotypes of mouse models expressing the Apert FGFR2 S252W mutation in neural crest-or mesoderm-derived tissues. *Bone*. 2014;63:101-109.

8. Martínez-Abadías N, Heuzé Y, Wang Y, Jabs EW, Aldridge K, Richtsmeier JT. FGF/FGFR signaling coordinates skull development by modulating magnitude of morphological integration: evidence from Apert syndrome mouse models. *PLoS One*. 2011;6(10):e26425. doi:org/10.1371/journal.pone.0026425

9. Holmes G, Basilico C. Mesodermal expression of Fgfr2 S252W is necessary and sufficient to induce craniosynostosis in a mouse model of Apert syndrome. *Dev Biol*. 2012;368(2):283-293. doi:10.1016/j.ydbio.2012.05.026

10. Holmes G, Rothschild G, Roy UB, Deng CX, Mansukhani A, Basilico C. Early onset of craniosynostosis in an Apert mouse model reveals critical features of this pathology. *Dev Biol*. 2009;328(2):273-284. doi:10.1016/j.ydbio.2009.01.026

11. McBratney-Owen B, Iseki S, Bamforth SD, Olsen BR, Morriss-Kay GM. Development and tissue origins of the mammalian cranial base. *Dev Biol*. 2008;322(1):121-132. doi:10.1016/j.ydbio.2008.07.016

12. Adams DC, Rohlf FJ, Slice DE. Geometric morphometrics: Ten years of progress following the 'revolution.' *Ital J Zool*. 2004;71(1):5-16. doi:10.1080/11250000409356545

13. Rohlf FJ, Slice D. Extensions of the Procrustes method for the optimal superimposition of landmarks. *Syst Biol*. 1990;39(1):40-59. doi:10.2307/2992207

14. Slice DE. Geometric morphometrics. *Annu Rev Anthropol*. 2007;36. doi:10.1146/annurev.anthro.34.081804.120613

15. Klingenberg CP. Size, shape, and form: concepts of allometry in geometric morphometrics. *Dev Genes Evol*. 2016;226(3):113-137. doi:10.1007/s00427-016-0539-2

16. Klingenberg CP, Monteiro LR. Distances and directions in multidimensional shape spaces: implications for morphometric applications. *Syst Biol*. 2005;54(4):678-688.

17. Zelditch ML, Swiderski DL, Sheets HD. *Geometric Morphometrics for Biologists: A Primer*. Academic Press; 2012.

18. Rohlf FJ, Corti M. Use of two-block partial least-squares to study covariation in shape. *Syst Biol*. 2000;49(4):740-753. doi:10.1080/106351500750049806

19. Mitteroecker P, Gunz P, Windhager S, Schaefer K. A brief review of shape, form, and allometry in geometric morphometrics, with applications to human facial morphology. *Hystrix*. 2013;24(1):59-66.

20. Mitteroecker P, Gunz P, Neubauer S, Müller G. How to explore morphological integration in human evolution and development? *Evol Biol*. 2012;39(4):536-553. doi:10.1007/s11692-012-9178-3

21. Klingenberg CP. Morphometric integration and modularity in configurations of landmarks: tools for evaluating a priori hypotheses. *Evol Dev*. 2009;11(4):405-421. doi:10.1111/j.1525-142X.2009.00347.x

22. Klingenberg CP. MorphoJ: an integrated software package for geometric morphometrics. *Mol Ecol Resour*. 2011;11(2):353-357.

23. Mitteroecker P, Bookstein F. The conceptual and statistical relationship between modularity and morphological integration. *Syst Biol*. 2007;56(5):818-836.

24. Lieberman DE, Hallgrímsson B, Liu W, Parsons TE, Jamniczky HA. Spatial packing, cranial base angulation, and craniofacial shape variation in the mammalian skull: testing a new model using mice. *J Anat*. 2008;212(6):720-735. doi:10.1111/j.1469-7580.2008.00900.x

25. Scott JH. The analysis of facial growth: II. The horizontal and vertical dimensions. *Am J Orthod*. 1958;44(8):585-589. doi:10.1016/0002-9416(58)90037-X

26. Scott JH. The analysis of facial growth: I. The anteroposterior and vertical dimensions. *Am J Orthod*. 1958;44(7):507-512. doi:10.1016/0002-9416(58)90083-6

27. Bastir M, Rosas A, O'Higgins P. Craniofacial levels and the morphological maturation of the human skull. *J Anat*. 2006;209(5):637-654. doi:10.1111/j.1469-7580.2006.00644.x

28. Hallgrimsson B, Lieberman DE, Young NM, Parsons T, Wat S. Evolution of covariance in the mammalian skull. In: *Novartis Foundation Symposium*. Vol 284. Chichester; New York; John Wiley; 1999; 2007:164.

29. Cohen Jr MM, Kreiborg S. A clinical study of the craniofacial features in Apert syndrome. *Int J Oral & Maxillofac Surg*. 1996;25(1):45-53. doi:10.1016/S0901-5027(96)80011-7

30. Richtsmeier JT, DeLeon VB. Morphological integration of the skull in craniofacial anomalies. *Orthod Craniofac Res*. 2009;12(3):149-158. doi:10.1111/j.1601-6343.2009.01448.x

31. Wilkie AO, Morriss-Kay GM. Genetics of craniofacial development and malformation. *Nat Rev Genet*. 2001;2(6):458-468. doi:10.1038/35076601

32. Rice R, Spencer-Dene B, Connor EC, et al. Disruption of Fgf10/Fgfr2b-coordinated epithelial-mesenchymal interactions causes cleft palate. *J Clin Investig*. 2004;113(12):1692-1700. doi:10.1172/JCI20384

33. Liu B, Rooker SM, Helms JA. Molecular control of facial morphology. In: *Semin Cell Dev Biol*. Vol 21. Elsevier; 2010:309-313. doi:10.1016/j.semcdb.2009.09.002

34. Holmes G, O'Rourke C, Motch Perrine SM, et al. Midface and upper airway dysgenesis in FGFR2-related craniosynostosis involves multiple tissue-specific and cell cycle effects. *Development*. 2018;145(19):dev166488. doi:10.1242/dev.166488

Table 1: Mouse models used in this sample

Sample	**Genotype**	**Number of specimens**	**Mutation**	**Cell type targeted by *Fgfr2* mutation**
Meso $^{+/+}$	*Mesp1Cre*$^{Tg/+}$*; Fgfr2*$^{+/+}$	20	None	None
NC $^{+/+}$	*Wnt1Cre*$^{Tg/+}$*; Fgfr2*$^{+/+}$	19	None	None
Fgfr2$^{+/+}$	*Ella-Cre*$^{Tg/+}$*; Fgfr2*$^{+/+}$	20	None	None
Meso$^{+/S252W}$	*Mesp1Cre*$^{Tg/+}$*; Fgfr2*$^{+/S252W}$	23	Conditional Apert syndrome FGFR2 S252W	Mesoderm-derived
NC$^{+/S252W}$	*Wnt1Cre*$^{Tg/+}$*; Fgfr2*$^{+/S252W}$	15	Conditional Apert syndrome FGFR2 S252W	Neural crest-derived
Fgfr2$^{+/S252W}$	*Ella-Cre*$^{Tg/+}$*; Fgfr2*$^{+/S252W}$	19	Full Apert syndrome FGFR2 S252W	All cells
Total		**116**		

Numbers	Descriptions
1 & 7	Most supero-anterior point of the maxilla accounting for the lateral part of the nasal aperture
2 & 8	Most postero-lateral point of the nasal bone
3 & 9	Most superior point of the infraorbital hiatus
4 & 10	Most distal point of the infraorbital hiatus
5 & 11	Most inferior point of the infraorbital hiatus
6 & 12	Intersection of zygoma with zygomatic process of temporal, taken on zygoma
13 & 14	Most posterior point of the anterior palatine foramen
15 & 18	Most medio-anterior point of the parietal
16 & 19	Most postero-medial point on the parietal
17 & 20	Most postero-lateral point on the parietal
21	Opisthion
24	Basion
22 & 25	Most infero-lateral point on the squamous occipital
23 & 26	The superior posterior point on the ectocranial surface of the occipital lateralis on the foramen magnum
27 & 28	Most antero-lateral point on the corner of the basioccipital

Table 2: Landmarks used in this study

Table 3: Procrustes distances among the different groups

Ploidy	*Fgfr*$^{+/S252W}$	*Meso*$^{+/S252W}$	*NC*$^{+/S252W}$	Nonmutants	P-value
Fgfr$^{+/S252W}$	0	**0.0773**	**0.0608**	**0.0910**	<.0001
Meso$^{+/S252W}$	0.0773	0	**0.0443**	**0.0369**	<.0001
NC$^{+/S252W}$	0.0608	0.0443	0	**0.0504**	<.0001

Table 4: Results of the PLS analyses: covariance and correlation values

2B-PLS analysis on Procrustes coordinates										
Specimens	**% Cov PLS1**	**Corr PLS1**	**P-value**	**% Cov PLS2**	**Corr PLS2**	**P-value**	**% Cov PLS3**	**Corr PLS3**	**P-value**	**RV coeffi-cient**
All	94.98	0.75	<.0001	3.35	0.60	<.0001	0.77	0.58	<.0001	0.46
Mutants	90.18	0.75	<.0001	7.67	0.76	<.0001	0.87	0.65	0.002	0.46
Nonmutants	51.98	0.70	<.0001	20.11	0.57	0.048	10.22	0.67	0.0001	0.27
2B-PLS analysis on regression residuals										
Specimens	**% Cov PLS1**	**Corr PLS1**	**P-value**	**% Cov PLS2**	**Corr PLS2**	**P-value**	**% Cov PLS3**	**Corr PLS3**	**P-value**	**RV coeffici-ent**
All	86.05	0.69	<.0001	9.90	0.60	<.0001	1.78	0.50	0.0003	0.35
Mutants	72.75	0.69	<.0001	21.98	0.68	<.0001	1.66	0.55	0.0473	0.35
Nonmutants	53.06	0.71	<.0001	21.63	0.60	0.0198	12.21	0.66	0.0010	0.30

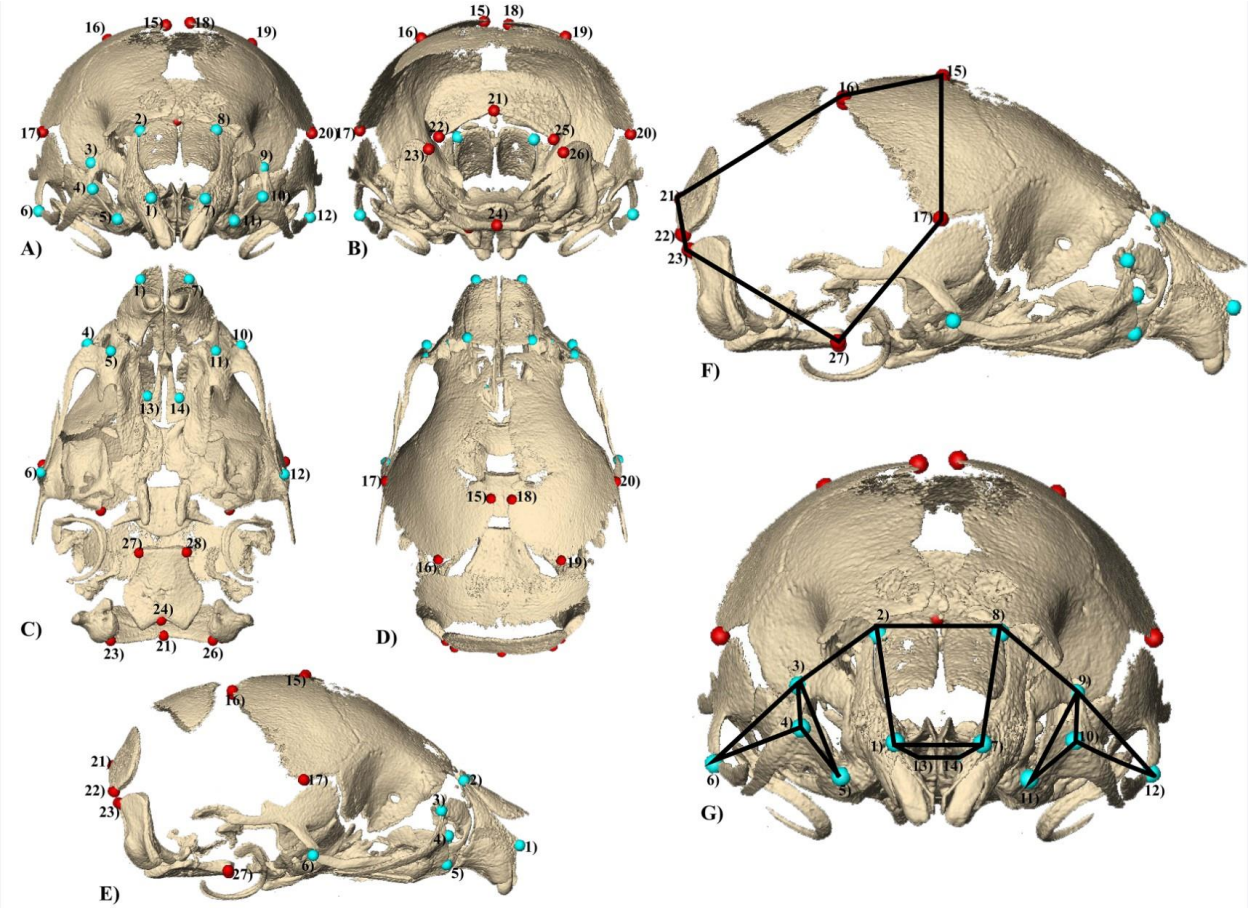

Figure 1: Illustration of the 28 3D cranial landmarks used in the study: A) Anterior cranial view; B) Posterior cranial view; C) Inferior cranial view; D) Superior cranial view; E) Lateral cranial view; F) Wireframe diagram of 14 neurocranial landmarks in lateral view; and G) Wireframe diagram of 14 facial landmarks in anterior view.

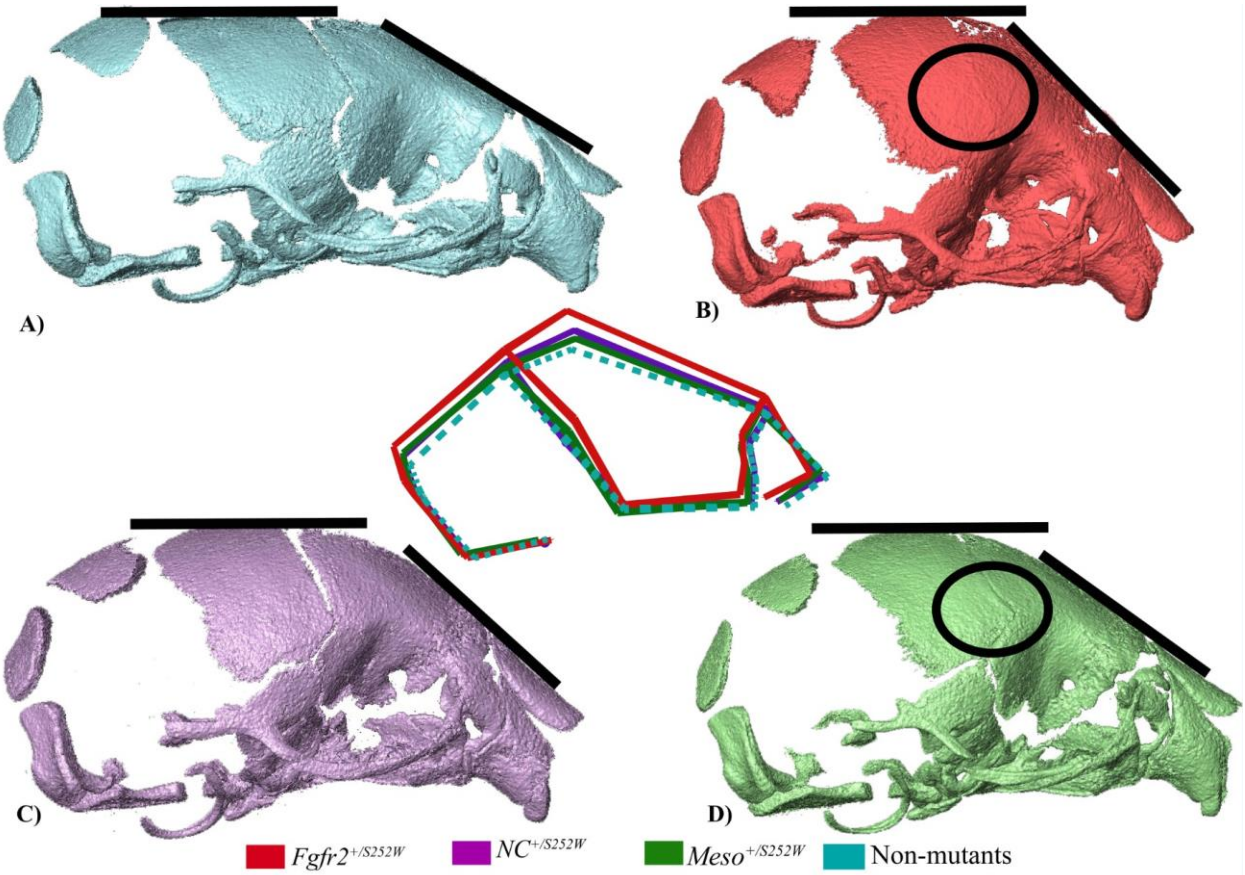

Figure 2: Isosurfaces of cranial mean shapes of the respective mouse models in lateral view: A) Non-mutants; B) *Fgfr2*$^{+/S252W}$ mutants; C) *NC*$^{+/S252W}$ mutants; D) *Meso*$^{+/S252W}$ mutants. The solid lines mark the changes in the lateral profile of the different groups illustrating the slope of the face in relation to the cranial vault shape. The ovals indicate closure of the coronal suture in the *Fgfr2*$^{+/S252W}$ and *Meso*$^{+/S252W}$ mice.

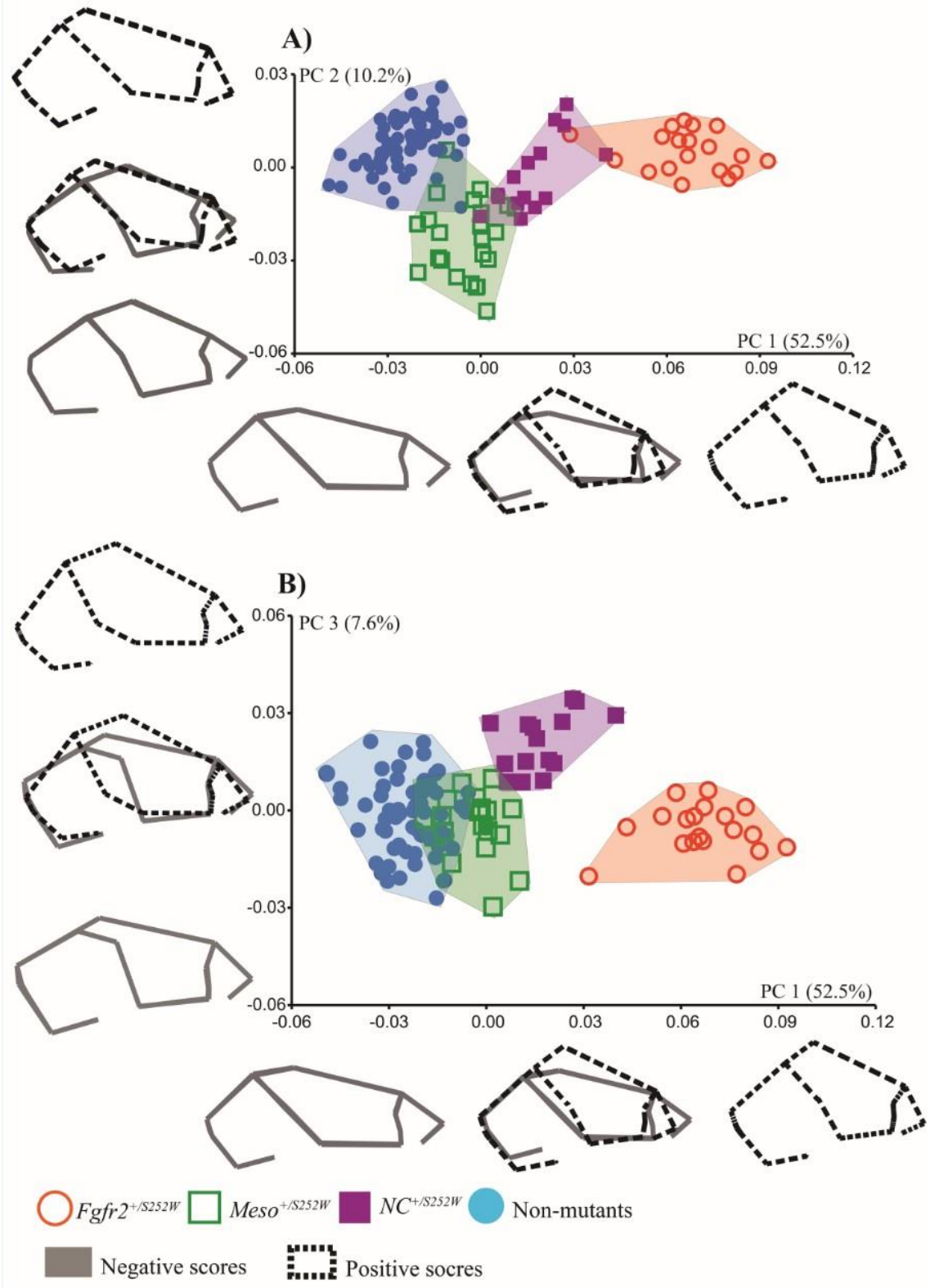

Figure 3: A) PC 1 vs PC 2 of all the cranial landmarks illustrating the shape variation across all the mouse strains in the sample; B) PC 1 vs PC 3. The wireframe diagrams of the shape changes along the negative and positive end of the PC axes are displayed in lateral view.

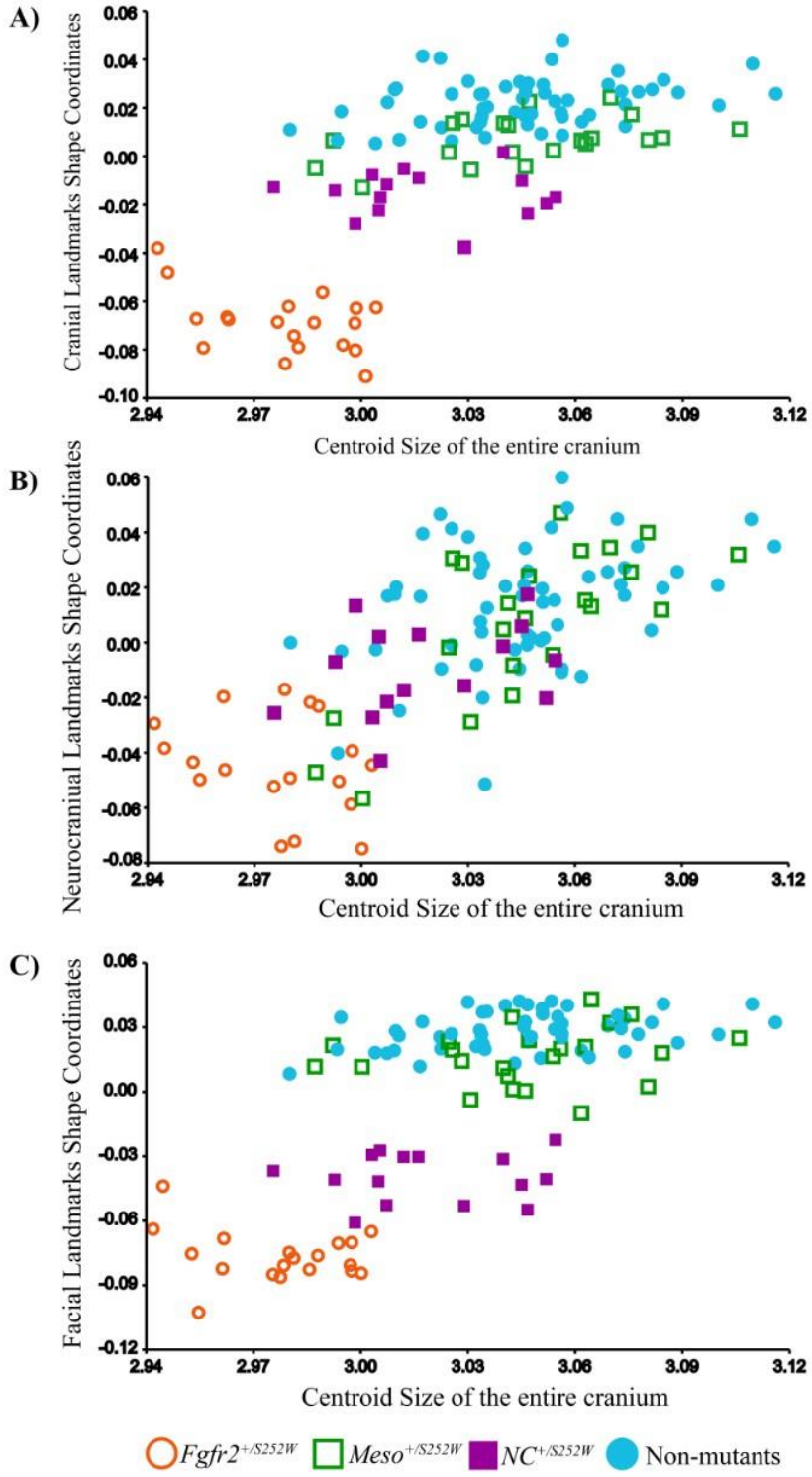

Figure 4: Multivariate regression analysis of shape on size: A) All 28 cranial shape coordinates on centroid size; B) 14 neurocranial shape coordinates on the cranial centroid size; and C) 14 facial shape coordinates on cranial centroid size.

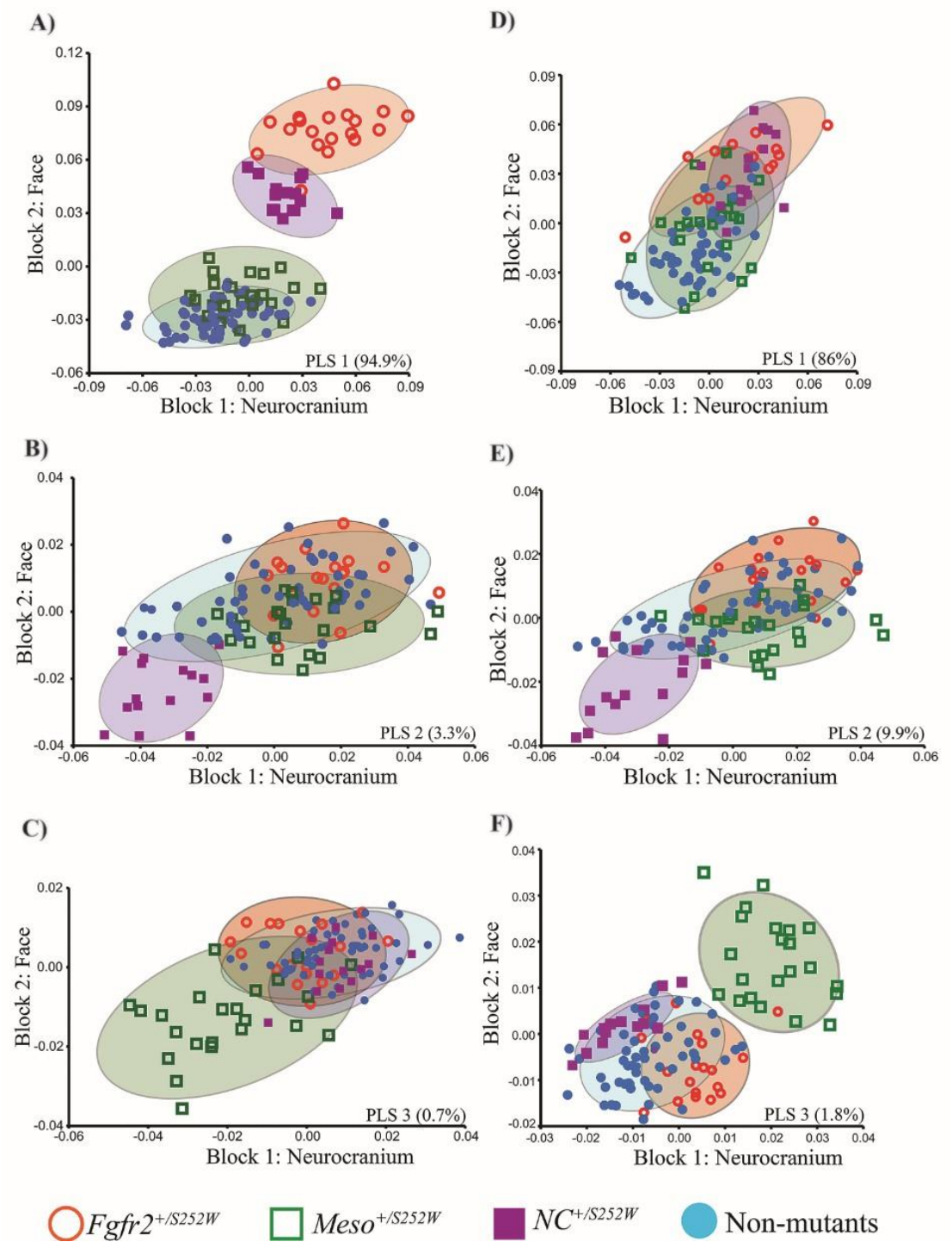

Figure 5: 2B-PLS plots of PLS 1, PLS 2, and PLS 3. A-C) 2B-PLS analysis without size correction, i.e. allometry, illustrating associated shape change between the mesoderm-derived regions of the neurocranium and neural crest-derived regions of the face; D-F) Size-corrected 2B-PLS analysis showing integrated shape changes between the mesoderm-derived regions of the neurocranium and neural crest-derived regions of the face.

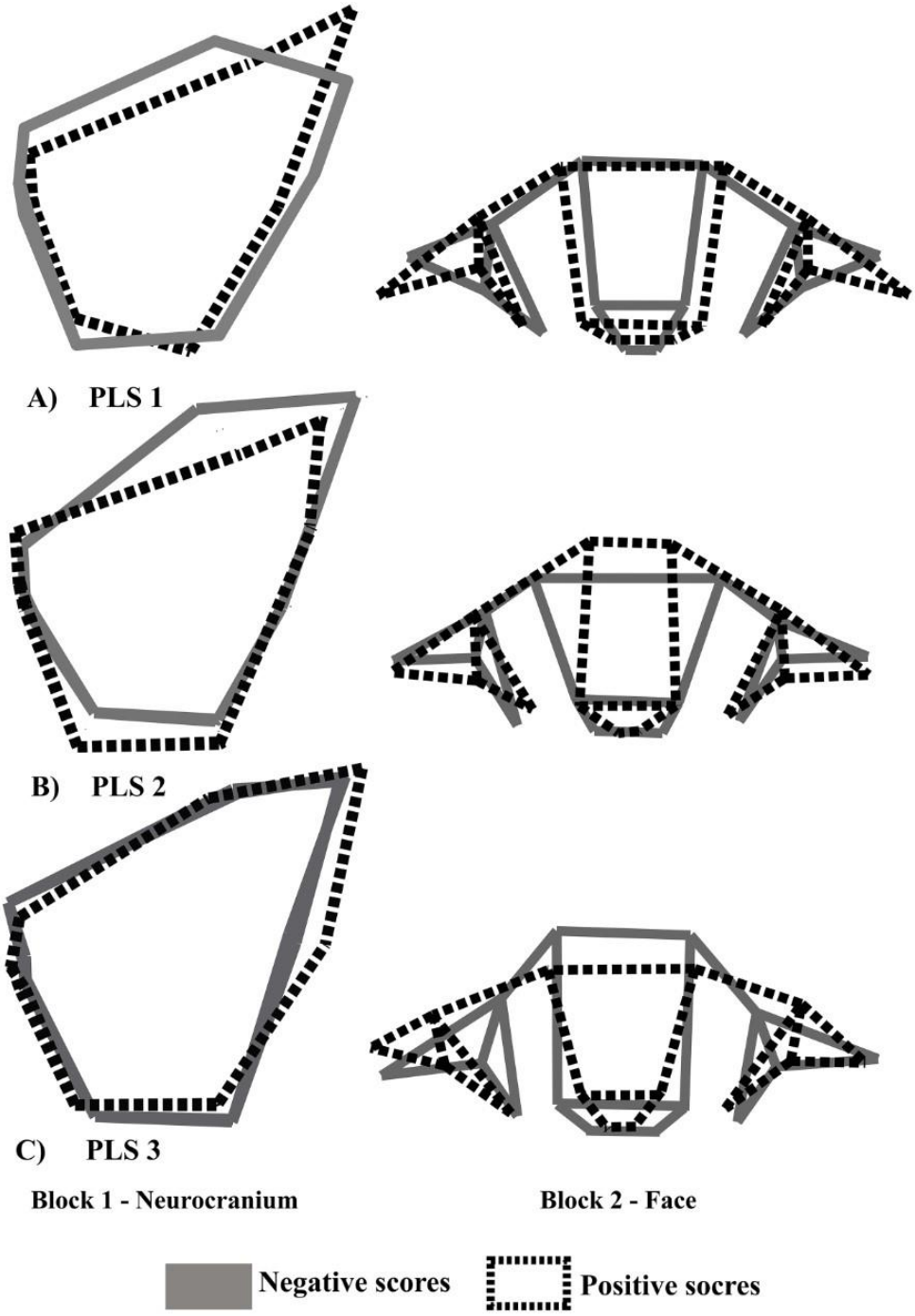

Figure 6: Wireframe diagrams illustrating the patterns of shape covariation between the neurocranium and face in the three PLS axes. A) Compares the integrated shape changes along the negative and positive scores of PLS 1. A supero-inferiorly high and anteriorly retracted cranial vault covaries with a medio-laterally narrow and anteriorly extended face; B) PLS 2 captures changes in the antero-superior part of the cranial vault, which covary with changes in the nasal-frontal junction of the snout; C) PLS 3 shows changes in the inferior part of the cranial vault associated with changes in the supero-inferior dimensions of the snout.

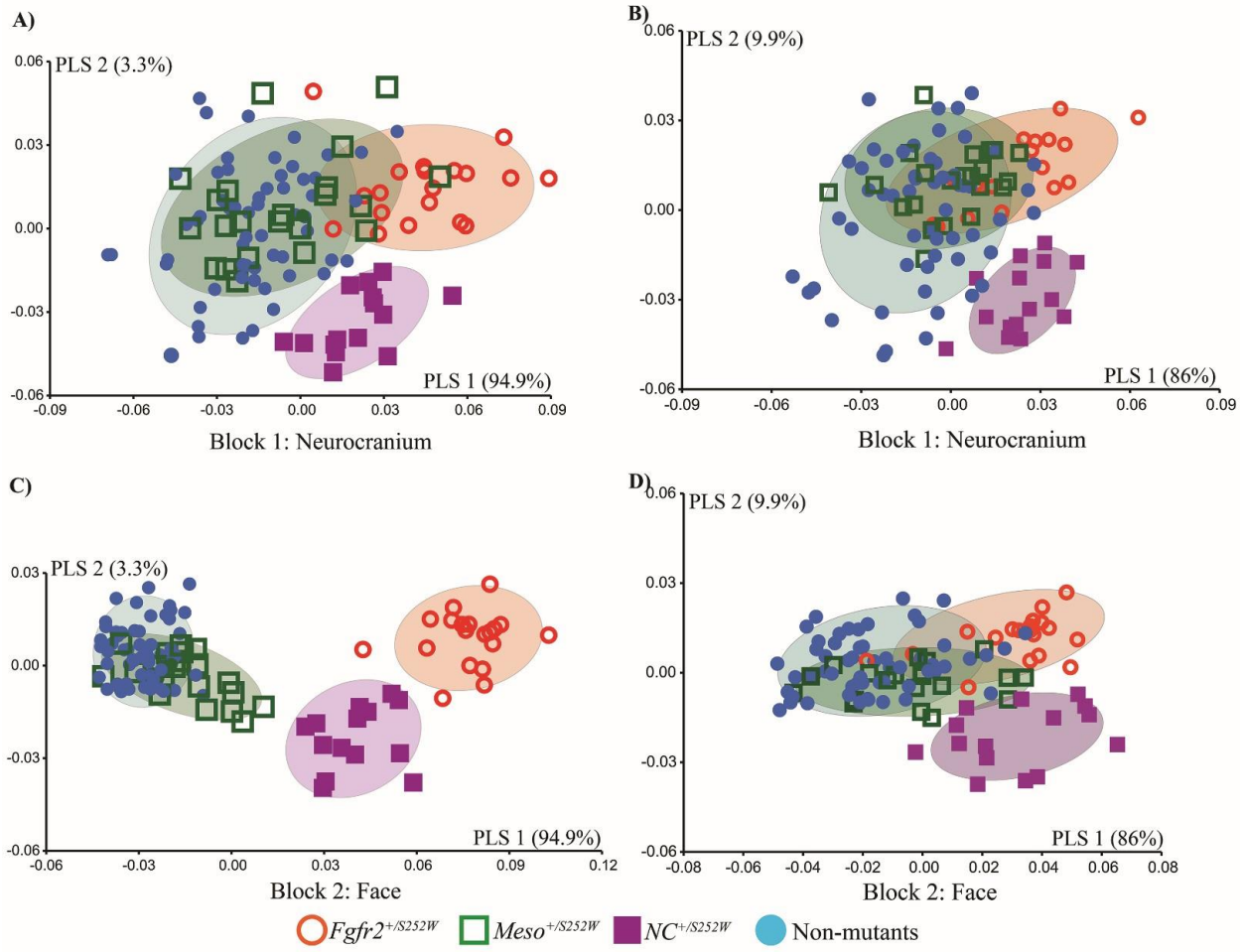

Figure 7: Modular shape variation in the neurocranium and face along PLS 1 vs PLS 2: A & C) 2B-PLS analysis without size correction on the neurocranial (A) and facial (C) components; B & D) 2B-PLS analysis with size correction, done on the regression residuals, on the neurocranium (B) and face (D).